

# Double and single side-band suppressed-carrier optical modulator implemented at 1320 nm using LiNbO<sub>3</sub> crystals and bulk optics.

Azad Siahmakoun<sup>1</sup> and Sergio Granieri  
Department of Physics and Applied Optics,  
Rose-Hulman Institute of Technology,  
Terre Haute, Indiana 47803.

Kenneth Johnson  
Naval Surface Warfare Center,  
Crane Division,  
Crane, Indiana 47522.

## ABSTRACT

We perform double sideband and single sideband suppressed-carrier modulators using a Mach-Zehnder interferometer in free space. Two bulk LiNbO<sub>3</sub> crystals are used to modulate the optical beam at 1319 nm in both branches of the interferometer. We present experimental results of the optical spectrum using heterodyne measurement technique. These results show maximum carrier and sideband suppression of 24 dB and 12 dB respectively for 1 GHz modulation frequency.

Keywords: Single side-band suppressed-carrier modulation, RF signal processing, electro-optic modulator

## 1- INTRODUCTION

Conventional intensity modulation involves a large carrier component while coherent single and double sideband suppressed-carrier have no carrier component. The suppression of an optical carrier leads to improvement of important characteristics of RF fiber optic link such as, linear dynamic range and noise figure<sup>1</sup>.

When a signal is sent over a fiber, chromatic dispersion causes each spectral component to suffer different phase shifts along the link. Thus, the power in the photodetector is severely affected producing degradation of the link performance. These penalties can be avoided by elimination of one sideband<sup>2</sup>.

In this paper we present the design of an electro-optic modulator based in a z-cut lithium niobate crystal together with its measured performance characteristics. We apply the developed electro-optic modulator in two modulation architectures: double and single sideband suppressed-carrier modulation. In the first application a modulator is used as phase modulator inside a Mach-Zehnder interferometer. In the second approach two modulators are placed between polarizers and are used as amplitude modulators.

In section 2, we experimentally demonstrate a double sideband optical modulation with suppressed carrier. In section 3 the suppression of one of the two modulation sidebands is discussed. Finally, details of the design and fabrication of the modulators are presented in section 4. Conclusions are given in section 5.

## 2- CARRIER SUPPRESSION

The experimental setup for carrier suppression is shown in Figure 1. A tunable solid-state laser provides the optical power for the input carrier at 1319 nm. A polarizing beam splitter (PBS) divides the input optical beam into the two arms of a Mach-Zehnder interferometer. A electro-optical modulator placed in one arm of the interferometer is used as phase modulator (see section 4 for more details). The optical field at each branch just before the second beam splitter (BS) may be expressed by

---

<sup>1</sup> Postal address: 5500 Wabash Ave., P. O. Box 192, IN 47803. E-mail: Azad.Siahmakoun@Rose-Hulman.edu

$$E_1(t) = E_1 \cos(\omega_c t), \quad (1a)$$

$$E_2(t) = E_2 \cos(\omega_c t + \Delta\phi), \quad (1b)$$

where  $E_1$ ,  $E_2$ , and  $\omega_c$  are the field amplitudes and the optical carrier frequency respectively, and  $\Delta\phi$  is the relative phase shift. A half-wave plate is placed between the laser source and the polarizing beam splitter. The relative intensity between the two beams is controlled by adjusting the angle of the slow axis of this plate.

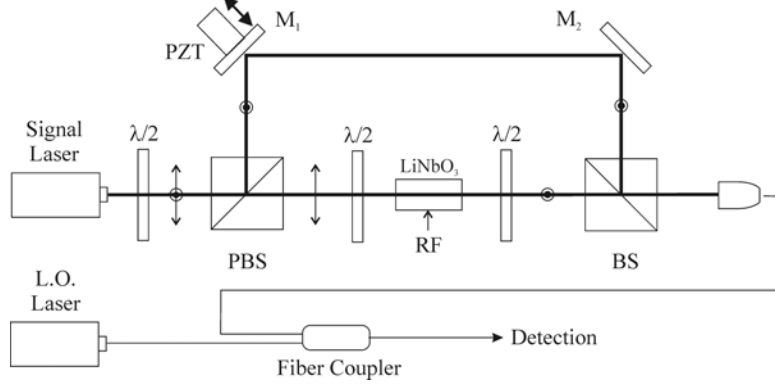


**Figure 1:** Experimental setup for carrier suppression

A linearly polarized light is passing through the crystal parallel to the principal axis  $X'$ , this is,  $45^\circ$  respect to the horizontal direction in the laboratory. Two half-wave plates provide the desired linear polarization direction at the input and output of the modulator. Using Eqs. (1), the output field after the second beam splitter can be written as

$$E(t) = E_1 \cos(\omega_c t) + E_2 \cos[\omega_c t + \Delta\phi' + \phi_m \cos(\omega_m t)] \quad (2)$$

where  $\Delta\phi'$  is overall constant phase shift between two arms, and  $\phi_m \cos(\omega_m t)$  the phase shift produced by the modulator with  $\omega_m$  the angular frequency of the applied RF signal. The modulation depth  $\phi_m$  is related to the crystal parameters through the half-wave voltage  $V_\pi$  as:  $\phi_m = \pi V_m / V_\pi$ , where the half-wave voltage is given by

$$V_\pi = \frac{\lambda}{n_0^3 r_{16}} \frac{d}{l}, \quad (3)$$

being  $\lambda$  the wavelength of the light, while  $l$  and  $d$  are the crystal length and the separation between two electrodes respectively. In order to find the condition to suppress the carrier component we expand Eq. (2) in terms of Bessel function as

$$\begin{aligned} E(t) = & E_1 \cos(\omega_c t) + E_2 J_0(\phi_m) \cos(\omega_c t + \Delta\phi') - \\ & - E_2 J_1(\phi_m) \{ \sin[(\omega_c + \omega_m)t + \Delta\phi'] + \sin[(\omega_c - \omega_m)t + \Delta\phi'] \} + \\ & + \text{high order terms,} \end{aligned} \quad (4)$$

where  $J_n()$  is the  $n$ -order Bessel function. The first two terms in this equation is the carrier component, and the second term is the first order side bands. As can be seen from Eq. (4), if the constant phase factor  $\Delta\phi' = \pm 180^\circ$ , and the amplitudes of the both beams are related by  $E_1 = E_2 J_0(\phi_m)$ , the carrier component is suppressed. The phase shift factor  $\Delta\phi'$  is set by varying the path difference between the arms of the Mach-Zehnder. Experimentally, the phase difference is adjusted by moving mirror  $M_1$  that is attached to a PZT actuator. The heterodyne method is used to shift the optical spectrum towards the electrical-frequency domain. A Lightwave 122 diode-pumped solid-state laser with 1319 nm wavelength provides the optical power for the input carrier. The band of interest is selected by mixing the optical output of the interferometer with a local oscillator using a fiber coupler. A NLK1356STB single-mode semiconductor laser with 20 mW optical power is used as local oscillator. Using this configuration, the coupler output is detected with a 10

GHz Ortel 4515A fiberoptic receiver. The output spectral components are visualized with a Tektronic 4202 RF spectrum analyzer. In order to demonstrate the feasibility of the proposal, we perform the carrier suppression by modulating the optical carrier with a sine wave at a frequency of 1GHz and power level of 30 dBm. Figure 2 shows the heterodyned optical spectrums centered at 220 MHz. The cases (a) through (c) correspond to different positions of the mirror  $M_1$ . The maximum and minimum power in the carrier component is consistent with  $\Delta\phi' = 0^\circ, \pm 180^\circ$  respectively. The measured power values for the carrier in (a) and (c) are  $-18.8$  dBm and  $-44.4$  dBm respectively. As can be seen from Figures 2(a) and 2(c), the direct RF term at 1GHz is attenuated as can be deduced from Eq. (4).

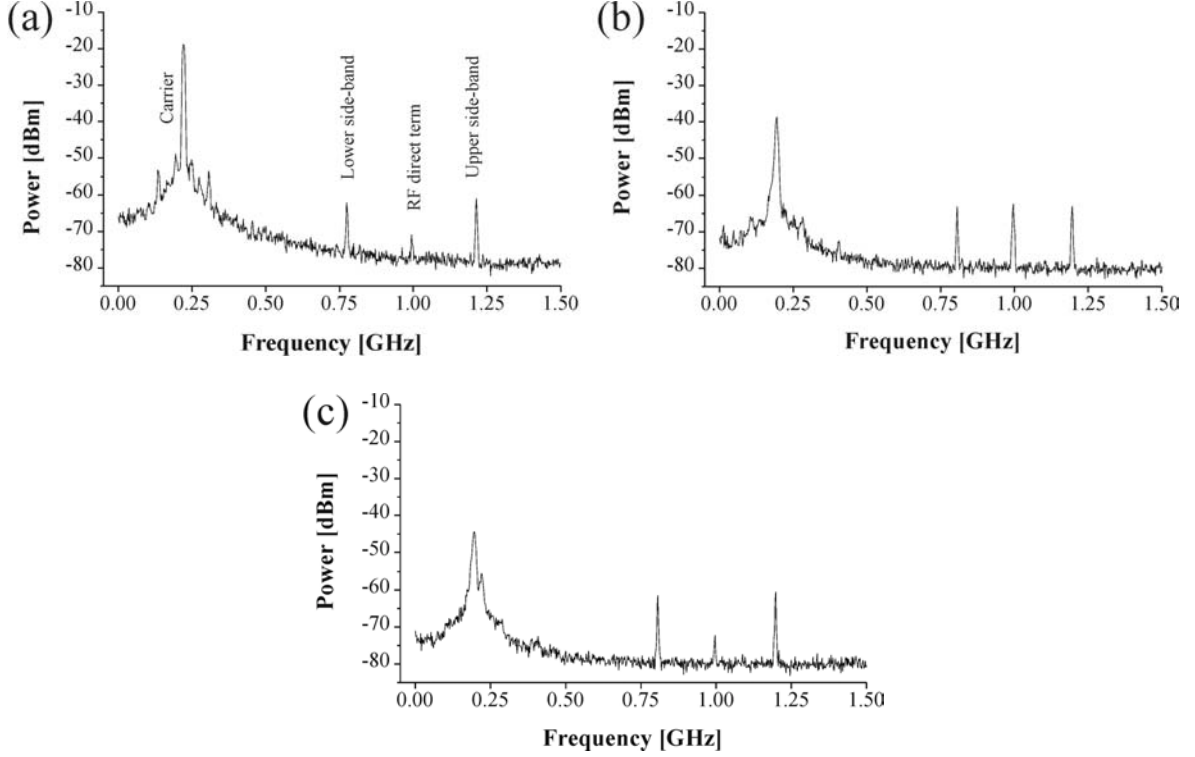


**Figure 2:** Heterodyned optical spectrum for (a)  $\Delta\phi'=0$ , (b)  $\Delta\phi'=\pm 90^\circ$ , and (c)  $\Delta\phi'=\pm 180^\circ$

### 3- SIDE-BAND SUPPRESSION

In order to suppress one of the side bands we perform an optical version of the Hartley microwave single side-band generator used in electrical modulation. Two amplitude-modulated signal are combined with suitable phase shift factors in the optical carrier as well as in the modulating RF signal. The experimental setup is shown in Figure 3. The main difference with the setup described in Figure 2 is that a second electro-optic modulator is placed in the Mach-Zehnder interferometer. The experimental setup is similar to the one presented in the last section, however, in the present case, both electro-optic modulators work as intensity modulators. The linear polarized light propagates through the crystal along the Z-axis with its plane of polarization initially inclined at  $45^\circ$  to the privileged directions  $X'$  and  $Y'$  as is shown in Figure 5(a) (see section 4 for more details). The total retardation between the S-components along both axes after the application of the voltage  $V$  is:  $\Gamma = \pi V / V_\pi$ , with the half-wave voltage given by

$$V_\pi = \frac{\lambda}{2n_0^3 r_{16}} \frac{d}{l}. \quad (5)$$

A half wave plate, placed after the polarizing beam splitter, is used to set properly the plane of linear polarization before each crystal. Notice that the polarizer  $P$ , placed after the second beam splitter, transmits only the X-component of the electric field. Thus, the field amplitude in each branch of the interferometer is

$$E(t) = E_0 \sin\left(\frac{\pi V_m}{2 V_\pi} \cos(\omega_m t)\right) \cos(\omega_c t + \phi_0) \quad (6)$$

where  $V_m \cos(\omega_m t)$  is the sinusoidal RF applied to the modulator,  $E_0$  is the input field amplitude and  $\phi_0$  is a constant phase factor. The optical signal given by Eq. (6) is intrinsically lack of carrier component. The carrier suppression in each arm of the interferometer is strongly related with the extinction ratio of the polarizer and the quality of the linear polarization state obtained from the PBS. The output field of the Mach-Zehnder can be written as

$$E(t) = E_0 \left[ \sin\left(\frac{\pi V_m}{2 V_\pi} \cos(\omega_m t)\right) \cos(\omega_c t) + \sin\left(\frac{\pi V_m}{2 V_\pi} \cos(\omega_m t + \Delta\Phi)\right) \cos(\omega_c t + \Delta\phi) \right] \quad (7)$$

where  $\Delta\Phi$  is the phase shift between both applied RF signals while  $\Delta\phi$  is the phase difference between carriers. The output field of Eq. (7) can be expanded in terms of the Bessel functions as

$$E(t) = E_0 J_1\left(\frac{\pi V_m}{2 V_\pi}\right) \left\{ \cos[(\omega_c + \omega_m)t] + \cos[(\omega_c + \omega_m)t + \Delta\phi + \Delta\Phi] + \right. \\ \left. + \cos[(\omega_c - \omega_m)t] + \cos[(\omega_c - \omega_m)t + \Delta\phi - \Delta\Phi] \right\} + \\ + \text{high order terms.} \quad (8)$$

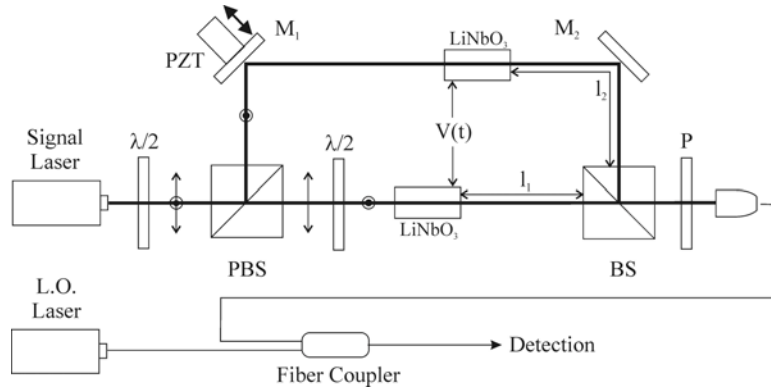


**Figure 3:** Experimental setup for side band suppression

As it can be noted from Eq. (8), setting the phase difference between carriers  $\Delta\phi$ , and between the electrical signals  $\Delta\Phi$ , as  $\pm 90^\circ$ , one of the sidebands will be eliminated. The  $90^\circ$  phase shift between electrical signals can be obtained by driving one modulator with the desired signal and the other with its Hilbert transform. Analogy to the last section, adjusting the position of mirror  $M1$  sets the phase difference between the carriers. The phase shift between the electrical signals is achieved by placing the modulators in an asymmetric path with respect to the beam splitter BS. The phase delay is set to  $\pm 90^\circ$  only for the appropriate frequency that satisfies

$$\omega_m = \frac{c\pi}{2|l_1 - l_2|}, \quad (9)$$

where  $l_1, l_2$ , are the distances from the modulators to BS, and  $c$  is the speed of light. The lasers are set to present a beating frequency of 3.755 GHz. The heterodyned output spectrum, showing a residual carrier component is shown in Figure 4. The bias voltage on the PZT driver is adjusted to suppress the lower sideband (case 4(a)) and the upper sideband (case 4(b)).

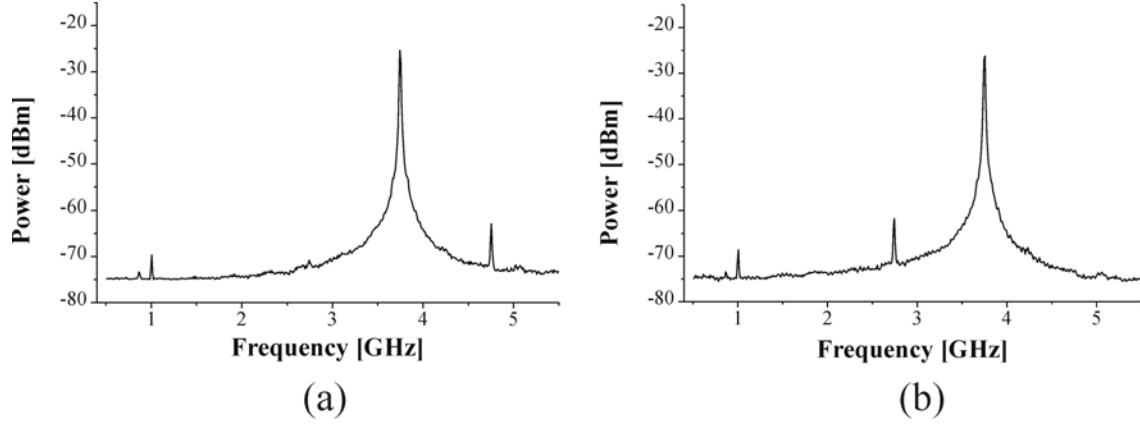


**Figure 4:** Heterodyne optical spectrum for two different positions of the mirror  $M_1$  that correspond to carrier phase differences of: (a)  $\Delta\phi=90^\circ$ , (b)  $\Delta\phi=-90^\circ$ .

#### 4- DESIGN AND CHARACTERIZATION OF ELECTRO-OPTIC MODULATORS

The component in which our modulators are based on is a lithium niobate ( $\text{LiNbO}_3$ ) crystal. This crystal has trigonal 3m symmetry. The samples are Z-cut with a pair of electrodes sputtered both sides. These electrodes are perpendicular to the X-axis as depicted in Figure 5(a). The dimensions of the samples along the X, Y, and Z directions are 9 mm, 9 mm, and 25 mm respectively.

In an anisotropic medium the refractive index changes with both the direction of polarization and propagation of the light. This index changes can be easily visualized by means of the index ellipsoid<sup>3</sup>. When an electric field is applied across the medium the principal axes directions are modified.

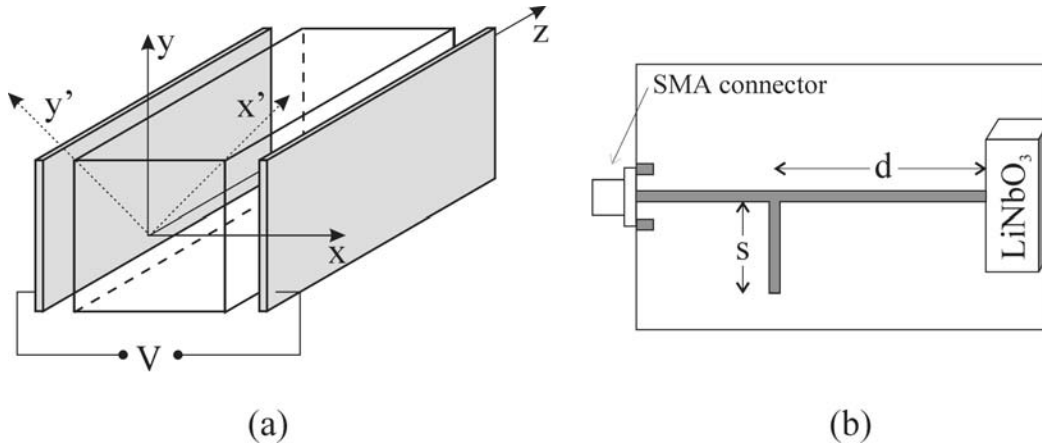


**Figure 5:** (a) Schematic of the  $\text{LiNbO}_3$  crystal showing the rotation of the principal axes under applied voltage. (b) Matching board: the lengths  $s$  and  $d$  related with the stub are chosen to achieve  $50 \Omega$  matching impedance at 1 GHz.

As can be seen from Figure 5(a), new axes  $X'$  and  $Y'$  results from a rotation of the axes  $X$  and  $Y$  about the  $Z$ -axis by an angle of  $45^\circ$  in the presence of an external electric field along the  $X$ -axis. The refractive indices along the new principal axis  $X'$  and  $Y'$  are

$$n_{x'}(E) = n_0 - \frac{1}{2} n_0^3 r_{16} E, \quad (10a)$$

$$n_{y'}(E) = n_0 + \frac{1}{2} n_0^3 r_{16} E. \quad (10b)$$

The crystal with the attached electrodes has an impedance with capacitive behavior when a RF signal is applied. In order to adjust the impedance between the crystal and 50  $\Omega$  transmission line a matching board is required. The matching is achieved by a microstrip with a tuned stub etched in a cooper board. Figure 5(b) shows the schematic of the board. The board material is RT/duroid 5870 1 oz. with a board height of 0.028in and a cooper thickness of 34  $\mu\text{m}$ . The accuracy of the matching was determined by calculating the voltage standing wave ratio (VSWR) for frequencies around 1 GHz. The VSWR is given by

$$VSWR = \frac{1 + |\Gamma|}{1 - |\Gamma|}, \quad (11)$$

where  $\Gamma$  is the reflection coefficient for the applied RF signal. To measure this coefficient, an RF signal was applied to the board-crystal through an RF-circulator sweeping the frequency around 1 GHz. The reflected signal out from the circulator was compared with the input signal using a HP 8720A Network Analyzer. Figure 6 shows the measured VSWR for frequencies from 0.8 to 1.1 GHz. If the board-crystal impedance matches exactly 50  $\Omega$ , the reflected signal and, consequently, the reflection coefficient should be zero. In this ideal case the VSWR=1 as is stated in Eq. (11). The minimum of the curve of Figure 6 indicates 0.95 GHz as the frequency for optimum impedance matching.

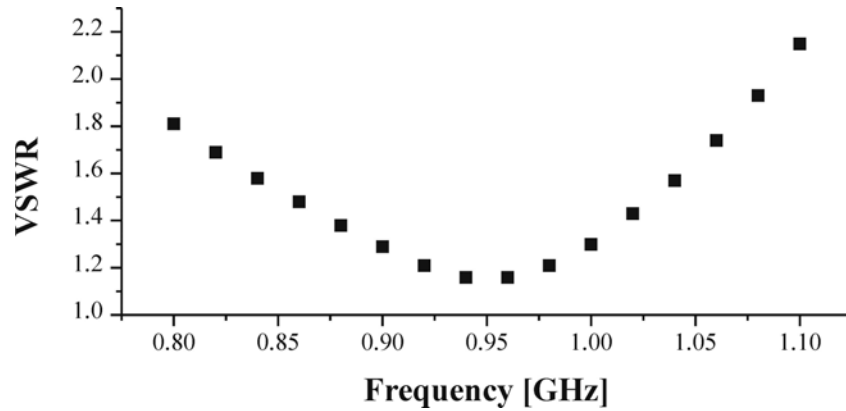


**Figure 6:** VSWR vs. frequency for the crystal with the 50  $\Omega$  matching board.

In order to test the electro-optic modulators we placed each between two crossed polarizers. A S-polarized beam, incident to the crystal, is parallel to the Y-axis (see Figure 5(a)). Thus, an amplitude modulated output signal is obtained when a sinusoidal RF signal is applied to the electrodes. To measure the dc- $V_{\pi}$  parameter, a dc voltage is applied to the electrodes while the output optical power is measured with a photodetector. Figure 7(a) shows the transmission of the amplitude modulator when a dc voltage from 0 through 2.5 kV is applied. From this curve a value of 2.2 kV for the dc- $V_{\pi}$  is calculated. The modulation efficiency is measured placing a quarter wave plate before the crystal in order to work in the linear response region. The RF signal from a Fluke 6061A synthesized signal generator was sent to the modulator through a Mini-circuit LZY-2 amplifier with 44 dB gain in the 0.5-1.1 GHz. bandwidth. The output RF power was measured using a 10 GHz Ortel 4515A photodetector and a Tektronic 2710 RF spectrum analyzer. The modulator is driven with a 1 GHz frequency single-tone RF signal. In figure 7(b) the output RF power versus input power from the signal generator from -22 dBm to -8 dBm is plotted.

## 5- CONCLUSIONS

The design and fabrication of a narrow band electro-optic modulator have been described. Several characteristics such as impedance matching, dc half-wave voltage and modulation efficiency are measured. In addition, two different optical modulation techniques have been implemented using the custom electro-optic modulator. Double and single sideband suppressed-carrier optical modulators are implemented using Mach-Zehnder interferometer and bulk optics in free space propagation. Suppression of the carrier by 25 dB and 12 dB for the sideband are achieved.

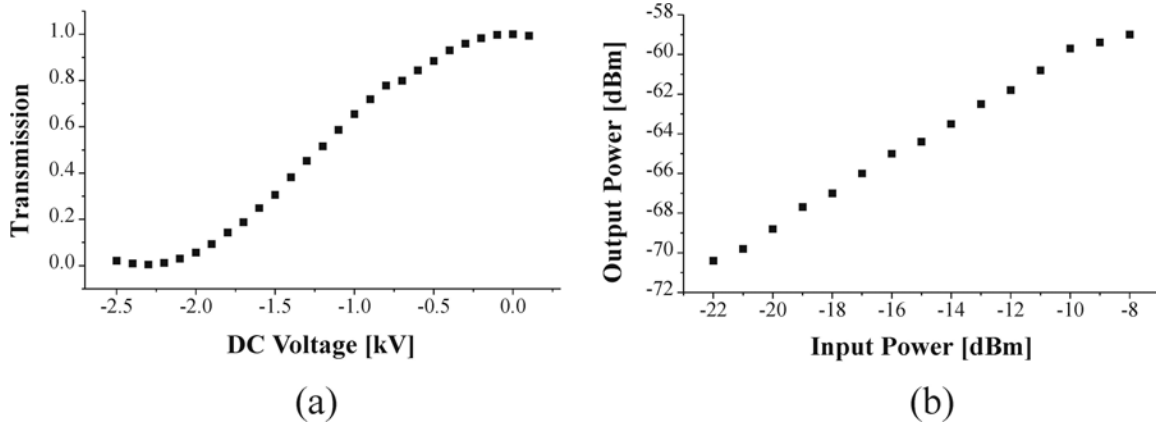


**Figure 7:** (a) Transmission versus DC voltage applied to the electrodes. (b) Output RF power versus input power from the signal generator.

### ACKNOWLEDGMENTS

The authors would like to thank Dan Purdy of Office of Naval Research for his support of this project under the contract number N00014-00-1-0782.

### REFERENCES

1. M. Farwell, W. Chang, and D. Huber, "Increased Linear Dynamic Range by Low Biasing the Mach-Zehnder Modulator", *IEEE Photonics Technol. Lett.*, **5**, 779-782, 1993.
2. K. Yonenaga, and N. Takachio, "A fiber chromatic dispersion compensation technique with an optical SSB transmission in optical homodyne detection systems", *IEEE Photonics Technol. Lett.*, **5**, 949-951, 1993.
3. A. Yariv, *Optical Electronics*, Chapter 9, Holt, Rinehart and Winston, New York, 1985.